Early immune responses are independent of RGC dysfunction in glaucoma with complement component C3 being protective

Jeffrey M. Harder[a], Catherine E. Braine[a], Pete A. Williams[a], Xianjun Zhu[b], Katharine H. MacNicoll[a], Gregory L. Sousa[a], Rebecca A. Buchanan[a], Richard S. Smith[a], Richard T. Libby[c], Gareth R. Howell[a,1], and Simon W. M. John[a,b,d]

[a]The Jackson Laboratory, Bar Harbor, ME 04609; [b]Howard Hughes Medical Institute, The Jackson Laboratory, Bar Harbor, ME 04609; [c]Flaum Eye Institute, University of Rochester Medical Center, Rochester, NY 14642; and [d]Department of Ophthalmology, Tufts University School of Medicine, Boston, MA 02111

Various immune response pathways are altered during early, predegenerative stages of glaucoma; however, whether the early immune responses occur secondarily to or independently of neuronal dysfunction is unclear. To investigate this relationship, we used the Wld^s allele, which protects from axon dysfunction. We demonstrate that DBA/2J.Wld^s mice develop high intraocular pressure (IOP) but are protected from retinal ganglion cell (RGC) dysfunction and neuroglial changes that otherwise occur early in DBA/2J glaucoma. Despite this, immune pathways are still altered in DBA/2J.Wld^s mice. This suggests that immune changes are not secondary to RGC dysfunction or altered neuroglial interactions, but may be directly induced by the increased strain imposed by high IOP. One early immune response following IOP elevation is up-regulation of complement C3 in astrocytes of DBA/2J and DBA/2J.Wld^s mice. Unexpectedly, because the disruption of other complement components, such as C1Q, is protective in glaucoma, C3 deficiency significantly increased the number of DBA/2J eyes with nerve damage and RGC loss at an early time point after IOP elevation. Transcriptional profiling of C3-deficient cultured astrocytes implicated EGFR signaling as a hub in C3-dependent responses. Treatment with AG1478, an EGFR inhibitor, also significantly increased the number of DBA/2J eyes with glaucoma at the same early time point. These findings suggest that C3 protects from early glaucomatous damage, a process that may involve EGFR signaling and other immune responses in the optic nerve head. Therefore, therapies that target specific components of the complement cascade, rather than global inhibition, may be more applicable for treating human glaucoma.

glaucoma | astrocytes | complement | EGFR | WLDS

Glaucoma is a common disorder characterized by the loss of retinal ganglion cells (RGCs) and degeneration of the optic nerve (1–3). Intraocular pressure (IOP) elevation is a major risk factor for developing glaucoma (4). Harmful IOP leads to changes in immune response pathways in nonneuronal cells, such as astrocytes and microglia/monocytes (5–9). Similar changes occur in many neurodegenerative diseases, including Parkinson's disease (10), Alzheimer's disease (11), and Huntington's disease (12). In glaucoma, immune responses are known to occur at predegenerative stages (5, 8), but key questions remain unanswered (2, 13–15). It is not known whether the earliest immune responses are protective or damaging, or which events irreversibly damage the optic nerve. Moreover, it is not known whether the immune responses are secondary to RGC dysfunction or occur independently, possibly as a more direct result of IOP elevation.

In glaucoma, an early insult to RGC axons occurs where they exit the eye in the optic nerve head (ONH) (16–20). Modeling shows that an increase in IOP inside the eye leads to increased strain in this critical region (21, 22). To understand the molecular responses occurring during glaucoma, gene expression profiles of human lamina astrocytes and ONH tissue from animal models

have been studied (reviewed in refs. 2, 15, 23). These studies identified changes in multiple genes/pathways related to immune responses, as well as structural and inflammatory changes in the ONH (8, 24, 25). The cause and impact of most of these changes in glaucoma remain to be determined, however.

To better understand the effects of high IOP in glaucoma, we used DBA/2J (D2) mice (26, 27). In D2 mice, high IOP causes RGC loss that can be prevented by IOP-lowering interventions (28–31). Importantly, glaucoma in D2 mice is an axonopathy, as evidenced by substantial RGC protection in the presence of the Wallerian degeneration slow allele (D2.Wld^s) (20). RGCs from D2.Wld^s mice can survive high IOP and have an intact pattern electroretinogram (PERG) (20). Given that PERG amplitude is a sensitive measure of RGC health (32, 33), Wld^s prevents very early changes. Confirming this effect here, we show that Wld^s also prevents other early features of glaucoma, RGC dendrite remodeling, and signs of axon stress.

Using D2.Wld^s mice as a tool to reduce complexity (specifically allowing the more direct study of high IOP on the ONH without potentially confounding effects of early RGC dysfunction), we compared ONH transcriptional profiles of D2.Wld^s mice with those of D2 mice at early predegenerative stages of disease. We discovered that early immune responses are not secondary to RGC dysfunction, but are more directly induced by elevated IOP. In addition, our data suggest that ONH astrocytes

---

Significance

Exactly how high intraocular pressure (IOP) initiates glaucoma is unknown. Immune responses occur early in glaucoma, but whether they are induced by high IOP or occur secondarily to retinal ganglion cell (RGC) dysfunction and molecular changes in neurons and glia remains unknown. This paper addresses these relationships and provides a deeper understanding of this very common neurodegeneration. Overall, our data suggest that early immune responses are independent of RGC dysfunction and thus are triggered as a more direct result of high IOP. Furthermore, early immune responses by astrocytes that involve complement C3 and EGFR signaling are beneficial.

activate beneficial processes, mediated by complement C3 and EGFR, in response to high IOP.

Materials and Methods

Mouse Strains, Breeding, and Husbandry. All experiments were conducted in accordance with the Association for Research in Vision and Ophthalmology statement on the use of animals in ophthalmic research and approved by The Jackson Laboratory's Institutional Animal Care and Use Committee. Mice were housed with a 14-h light/10-h dark cycle under previously described conditions (34). DBA/2J (D2), DBA/2J-$Gpnmb^+$/SjJ (D2-$Gpnmb^+$), and DBA/2J.BOla-Wld^s/Sj strain (D2.Wld^s) have been described previously (35–37). Mice were obtained from either The Jackson Laboratory production facility or the S.M.W.J. laboratory research colony. The S.M.W.J. laboratory research colony is periodically crossed with mice from The Jackson Laboratory production facility to prevent genetic drift.

To generate D2.$C3^{-/-}$ mice, $B6;129S4-C3^{tm1Crr}$/IJ mice (JAX repository 003641) were backcrossed to the D2 strain for at least 10 generations and then intercrossed.

Iris Disease and IOP Measurement. D2 mice develop elevated IOP and glaucoma subsequent to an iris disease (27, 36). In all D2 glaucoma experiments, the progression of the iris disease and IOP in mutant or drug-treated mice were compared with that in control D2 mice using previously described methods (26, 38). In each experiment, iris disease and IOP were assessed in 40 eyes per genotype or treatment. Iris disease was assessed at 2-mo intervals starting at age 6 mo until completion of the experiment. IOP was measured at 45-d intervals beginning at age 8.5–9 mo until completion of the experiment. Statistical analysis was performed using Student's t test.

Assessment of Optic Nerve Damage. The method of preparing, staining, and analyzing optic nerves for damage has been previously described and validated (5, 8, 20, 27, 34, 39). In brief, cross-sections of optic nerve are stained with paraphenylenediamine (PPD), which stains all myelin sheaths but darkly stains the axoplasm of injured or dying axons. This differential staining provides a very sensitive marker of axon damage, allowing the identification of individual damaged axons within a generally healthy nerve. The degree of nerve damage is determined based on readily distinguishable differences in the extent of axon damage. Nerves with no or early (NOE) glaucoma have healthy axons (i.e., intact myelin sheaths and clear axoplasm). They have no morphologically detectable glaucomatous damage, but some are at early molecular stages of glaucoma (5, 8). Moderately (MOD) affected nerves have readily detectable degenerating axons, as marked by darkly stained axoplasm; however, the majority of axons are still healthy. Severely (SEV) affected nerves have extensive axon damage throughout the nerve and obvious axon loss. Axon numbers are significantly different between optic nerves of each damage level (39).

To determine whether optic nerve damage levels are dependent on genotype or drug treatment, the proportions of each damage level and condition were compared using Fisher's exact test, with $P < 0.01$ considered significant. The sample size for each experiment was as follows: 12-mo-old Wld^s homozygotes, $n = 80$; 10-mo-old $C3^{+/+}$, $n = 45$; 10-mo-old $C3^{-/-}$, $n = 47$; 12-mo-old $C3^{+/+}$, $n = 52$; 12-mo-old $C3^{-/-}$, $n = 39$; 10-mo-old AG1478-treated, $n = 48$; 10-mo-old vehicle-treated, $n = 38$; 10-mo-old untreated, $n = 42$. When multiple conditions were included, individual comparisons were made using Fisher's exact test, and Bonferroni-corrected P values were considered for significance. Similar significant results were obtained when χ^2 tests were applied ($P < 0.01$ for all comparisons).

Nissl Staining of Whole-Mount Retinas and Ganglion Cell Layer Cell Counting. For Nissl staining, eyes were enucleated and fixed in 4% PFA overnight. Whole retinas were then dissected from the eye, placed in 1:1 alcohol:chloroform overnight, and rehydrated through a serial alcohol gradient. Retinas were washed once in distilled water and stained for 15 min in 0.1% cresyl violet in distilled water before being differentiated in 95% alcohol, dehydrated in 100% alcohol, and cleared in xylene. Retinas on slides were mounted with Fluoromount, coverslipped, and sealed with nail polish. Nissl-stained retinas were imaged using an upright light microscope.

Anterograde Axon Transport. Mice were injected intravitreally at age 12 mo with 1 μL (1 mg/mL in 0.1 M sterile phosphate buffer) Alexa Fluor 594-cholera toxin subunit B using a Hamilton syringe with a 33-gauge needle. After 48 h, mice were anesthetized and euthanized via 4% PFA cardiac perfusion. Brains were submersion-fixed in 4% PFA for 24 h after perfusion, rinsed in PBS, and cryoprotected in a 30% sucrose solution for 24 h. Brains

were then cryoembedded in optimal cutting temperature (OCT) compound and sectioned at 12–16 μm along the coronal plane. Alexa Fluor 594 was visualized using a Leica SP5 confocal microscope. Axon transport was assessed in at least three cross-sections of the central portion of the superior colliculus and was deemed normal when no differences were observed between the test eye and the D2-$Gpnmb^+$ control eyes. Ten eyes (10 hemispheres from 5 brains) were assessed for each genotype.

Diolistic Labeling and Morphological Analysis. Using a Helios gene gun system (Bio-Rad), flat-mounted retinas were labeled with DiO/DiI bullets, and RGCs were selected and analyzed as described previously (40). At age 9 mo, 12 eyes were labeled for each mouse strain (D2, D2-$Gpnmb^+$, and D2.Wld^s). The sample size was sufficient to reproduce the previously reported differences in dendrite morphology and mean dendritic field area in D2 and D2-$Gpnmb^+$ mice at age 9 mo using previously described methods (40).

6-Carboxyfluorescein Diacetate Cell Tracking. Splenocytes were labeled using 6-carboxyfluorescein diacetate (6-CFDA; Invitrogen) via intrasplenic injection, as described previously (5). At 72 h postinjection, mice were euthanized, eyes were harvested, and retinas and ONHs were dissected and fixed in 4% PFA and flat-mounted on glass slides. 6-CFDA was visualized immediately using a Leica SP5 confocal microscope. ONHs from 10 eyes were assessed for each genotype.

Preparation of Eyes for Gene Expression Profiling. Gene expression profiling was performed on 11-mo-old female mice, comparing profiles of three eyes from female D2.Wld^s mice and three eyes from D2 mice with no glaucoma with profiles of three eyes from age- and sex-matched, D2-$Gpnmb^+$, no-glaucoma controls (37). To obtain tissue for RNA sequencing, following euthanasia, eyes were enucleated cleanly with a small section of optic nerve attached. Each eye was dissected free in PBS, and the cornea, lens, and sclera were removed. The optic nerve was cut from the retina, preserving the ONH to just behind the myelin transition zone (20, 41), and placed in Buffer RLT (Qiagen). Dissections were completed within 5 min from the time of euthanasia. The corresponding retro-orbital portion was assessed for axon damage by PPD staining. Only eyes with no nerve damage (NOE) were selected for RNA sequencing. All eyes from D2-$Gpnmb^+$ mice had no optic nerve damage.

Primary Astrocyte Cultures. Here 3-d-old pups from D2.$C3^{+/-}$ intercross matings were euthanized and their cortices dissected out into glial dissection solution composed of tissue culture-grade water containing 10% HBSS (Gibco 14170; Invitrogen), 1% Hepes (Gibco 15630; Invitrogen), and 1% Pen/Strep (Gibco 15140; Invitrogen). Meninges were removed, and the remaining cortical tissue was trypsinized (HyClone Trypsin 0.25%; SV30031.02; Thermo Fisher Scientific) for 15 min at 37 °C. The reaction was inhibited with the addition of serum containing cortex glial medium (CGM) formulated with 1× MEM (Gibco 11095; Invitrogen) containing 10% heat-inactivated horse serum (Gibco 26050070; Invitrogen), 0.06% D-(+)-glucose, and 1% penicillin/streptomycin. The digested tissue was triturated, and the cellular suspension was passed through a 100-μm cell strainer. The suspension was plated in poly-D-lysine (0.1 mg/mL poly-D-lysine hydrobromide; Sigma-Aldrich P7886)-coated T25 flasks. Media was changed at 24 h after plating and every other day thereafter. Each media change consisted of the application of fresh CGM following two washes with 1× DPBS (Gibco 14190; Invitrogen). Cells were allowed to grow at 37 °C for 8 d before being passaged.

Astrocyte Culture Immunofluorescence. After passage, cells were plated in CGM on poly-D-lysine–coated 35-mm optical bottom culture dishes (P35GC-1.5–14-C; MatTek) until adherent (a minimum of 24 h). Primary astrocytes from 5-d-old male D2.$C3^{-/-}$ and D2.$C3^{+/+}$ pups were assessed for C3 expression by immunofluorescence (three pups per genotype). Cells were washed three times with 1× DPBS (Gibco 14190; Invitrogen), fixed for 15 min at room temperature in 2% PFA, and permeabilized by the application of 0.1% Triton in 1× PBS for 5 min. Cells were then blocked in 3% BSA/normal goat serum and 0.2% Tween in 1× PBS before the application of primary antibodies in 0.2% BSA/Triton X-100 in 1× PBS. Primary antibodies used were chicken anti- glial fibrillary acidic protein (GFAP; ab4674, 1:500; Abcam), rabbit anti-IBA1 (016–20001, 1:500; Wako), and rat anti-C3 (ab11862, 1:200; Abcam). Following either a 2-h incubation at room temperature or an overnight incubation at 4 °C, cells were washed in 1× PBS for 30 min. Cells were incubated in secondary antibodies (1:1,000; Invitrogen) for 30 min. Cells were rinsed in 1× PBS and mounted using Aqua-Poly/Mount coverslipping medium (18606–02; Polysciences). Fluorescent signal was detected using a Zeiss Axio Observer inverted microscope.

Preparation of Astrocytes for Gene Expression Profiling by FACS. Cortical astrocytes were cultured from three 5-d-old male $D2.C3^{-/-}$ and three 5-d-old male $D2.C3^{+/+}$ pups and purified using FACS. At 17 d after plating, astroglial cultures were harvested (HyClone Trypsin 0.25%; Thermo Fisher Scientific) and resuspended in FACS buffer and HBSS (Gibco 14025; Invitrogen) supplemented with 2% BSA (A7906; Sigma-Aldrich) and containing 1 U/μL SUPERase In RNase Inhibitor (Ambion AM2694; Life Technologies). The cells were centrifuged at 1,305 × g for 5 min and suspended in 50 μL of fresh FACS buffer. The cells were then stained for 1 h at 4 °C with 1:500 chicken anti-GFAP (ab4674; Abcam) to label astrocytes and 1:500 rabbit anti-IBA1 (016–20001; Wako) to label myeloid-derived cells. The cells were washed again and then incubated with 1:1,000 dilutions of donkey anti-rabbit 647 (A31573; Invitrogen) and goat anti-chicken (A11039; Invitrogen) for 30 min at 4 °C. Samples were centrifuged and washed three more times before being suspended in 200 μL of FACS buffer and sorted on an LSR II digital cell analyzer (BD Biosciences). Purified astrocytes, expressing high levels of GFAP and IBA1-negative, were sorted into RLT Buffer (79216; Qiagen) and stored at −80 °C.

Gene Expression Profiling by High-Throughput RNA Sequencing. ONH samples from D2.Wld^s and D2.$Gpnmb^+$ mice or astrocytes isolated and purified from D2.$C3^{-/-}$ and D2.$C3^{+/+}$ mice were homogenized by syringe in Buffer RLT from an RNeasy Micro Kit (Qiagen). For each sample, total RNA was isolated according to the manufacturer's protocol (Qiagen), and quality was assessed using an Agilent 2100 Bioanalyzer and an RNA 6000 Pico LabChip assay. Sequencing libraries were constructed using Ovation RNA-Seq V2 (NuGen) and TruSeq DNA V2 (Illumina) sample prep kits. Here 5 ng of starting RNA was used, and DNA was sheared to 300–400 bp. Quality control of all libraries was performed using an Agilent 2100 Bioanalyzer and DNA 1000 chip assay. The average insert size for the libraries was ~350 bp. To ascertain the amount of library produced, quantitative PCR was performed using the KAPA Library/Illumina GA/ABI Prism quantitation kits (Kapa Biosystems). Libraries were then clustered on an Illumina cBot, which allows the library to bind to the adapters on the flow cell. The flow cell was then placed in the Illumina HiSeq 2000 cell sequencer for sequencing.

Analysis of Gene Expression Data. The open-source Galaxy software platform was used for the analysis of RNA sequencing (RNA-seq) data. Galaxy is a curated suite of tools for performing RNAseq analysis (42). The Groomer tool was used to assess the quality of the FASTQ-formatted data from the Illumina-supplied data pipelines. Groomer parsed the sequencer output and calculated summary statistics for base quality scores and nucleotide distributions across reads. The Tophat tool was used to align RNA reads to the genome. Tophat is an implementation of the Bowtie alignment tool specifically designed for RNA-seq and optimized for paired-end sequencing. The output, in sequence alignment map format, was assembled into transcripts using the Cufflinks tool. Cuffdiff was used to identify differentially expressed (DE) transcripts and genes between sample groups. DE genes were determined using a probability of $P < 0.1$.

RNA in Situ Hybridization. $C3$, $C1qa$, and Vim riboprobes were transcribed from cDNA clones (clones 5038612, 3592169, and 6415629, respectively; Thermo Fisher Scientific). Plasmids were isolated using the Qiagen Plasmid Mini Kit and digested with EcoR1 ($C3$) and Sal1 ($C1qa$ and Vim). Digested plasmids were purified via phenol-chloroform extraction, and antisense digoxigenin-labeled and FITC-labeled riboprobes were generated in vitro with T7 polymerase. SP6 polymerase was used to generate control sense riboprobes, which produced no signal when tested.

Eyes were enucleated from six 10.5-mo-old DBA/2J mice following cardiac perfusion with 4% PFA. The tissues were submersed in 4% PFA overnight, washed for 15 min with 1× PBS, and then transferred to 30% sucrose solution. Following sucrose saturation, eyes were cryoembedded in OCT and stored at −80 °C. RNA in situ hybridization was done using 10-μm cryostat sections. Sections were incubated overnight at 65 °C with 1 μg/μL of both a digoxigenin-labeled probe and an FITC-labeled probe in 50% Hybridization Solution (H7140; Sigma-Aldrich) and 50% formamide (AM9342; Ambion). Hybridized mRNA was detected using the Cy-3 and Fluorescein Tyramide Signal Amplification Systems (NEL744B001KT and NEL741001KT, respectively; PerkinElmer). Following in situ hybridization, sections were incubated with DAPI (D1306; Invitrogen) and mounted with Aqua-Poly/Mount Coverslipping Medium (18606–02; Polysciences). Fluorescent signal was detected using a Leica SP5 or SP8 confocal microscope.

AG1478 Administration. The selective EGFR inhibitor AG1478 (T-7310; LC Laboratories) was administered by a mini osmotic pump (model 2004; Alzet). Custom model 2004 pumps were used, which allowed 6 wk of delivery; batch characteristics were specifically selected to allow this. Mice were anesthetized using isoflurane, and the pumps with attached Lynch coils were implanted s.c. via a 1-cm lateral midscapular incision at age 7 mo and replaced every 39 d. Control mice with pumps containing only vehicle were treated in exactly the
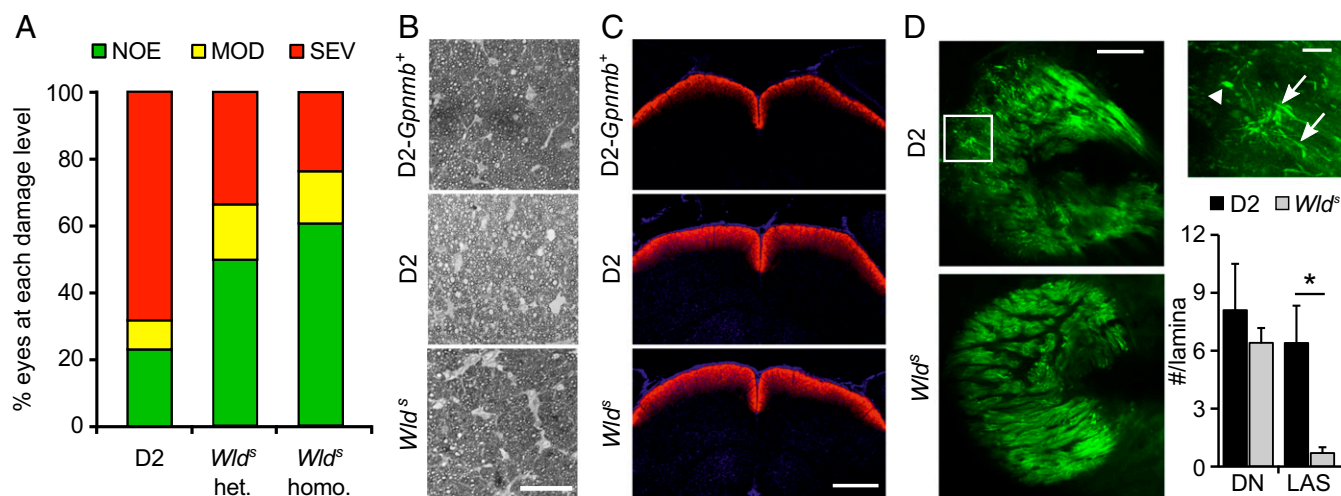

Fig. 1. Wld^s homozygosity is no more protective than Wld^s heterozygosity. (*A*) The Wld^s allele protected from glaucomatous optic nerve damage at age 12 mo [$P < 0.003$, χ^2 test of independence comparing heterozygous (het) or homozygous (homo) mice with standard D2 littermates], but increasing gene dosage was not significantly more protective. Bars represent the distribution of optic nerve damage by genotype: no or early (NOE; healthy clear axons with PPD stain), moderate (MOD; darkly stained axons, with PPD stain indicating damage, but with the majority of axons healthy), or severe (SEV; majority of axons damaged/lost). D2 and het data were reported previously (20). (*B*) Examples of PPD-stained cross sections of retro-orbital optic nerves showing similar staining in D2-$Gpnmb^+$ no-glaucoma control compared with D2 (NOE) and D2.Wld^s homo (NOE). (*C*) No differences were detected in the transport of anterograde tracer Alexa Fluor 594-cholera toxin subunit B (red) to the superior colliculus (SC) among NOE eyes from D2 mice (*Middle*), D2.Wld^s (*Lower*), and no-glaucoma D2-$Gpnmb^+$ control eyes (*Upper*). Axon transport was assessed at age 12 mo. (*D*) ONH axon integrity was assessed in D2 and D2.Wld^s eyes using cyan fluorescent protein expression driven from a Thy1 promoter (*Materials and Methods*). In 9-mo D2 eyes (*Upper Left*), local axonal swellings (LAS; *Upper Right*, arrows) and dystrophic neurites (DN; *Upper Right*, arrowhead) were observed, as reported previously (20); however, the number of local axonal swellings was greatly reduced in D2.Wld^s eyes (*Lower Right*; $P < 0.01$). (Scale bars: 50 μm in *C*; 500 μm in *D*.)
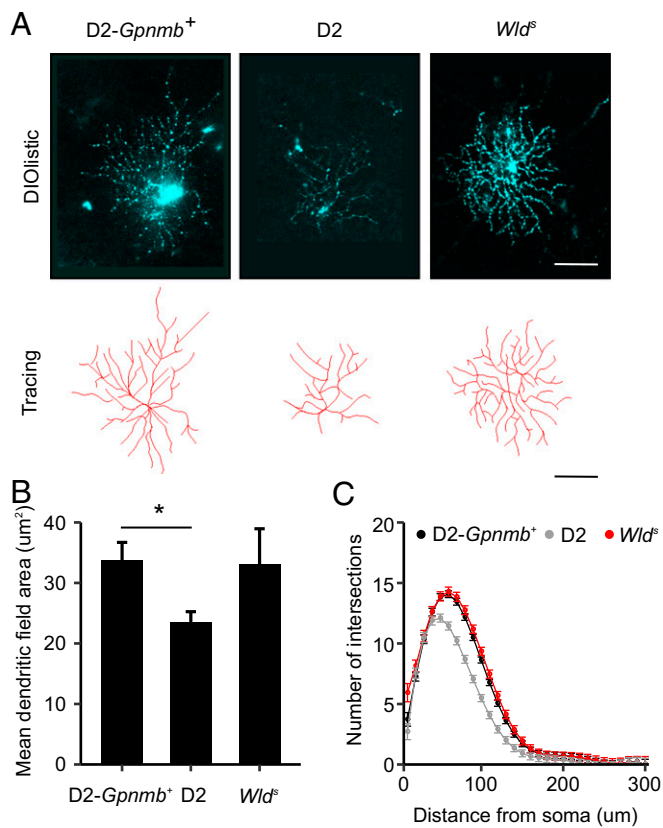
Fig. 2. RGCs from D2.*Wld^s* eyes do not show dendrite remodeling. (*A*) At 9 mo, retinal cells were filled and RGCs identified based on axons projecting to the ONH and dendrites traced (*Materials and Methods*). (*B* and *C*) There was no statistical difference in the mean dendritic field area (*B*) or the number of intersections from a Sholl analyses (*C*) between RGCs from D2.*Wld^s* and D2.*Gpnmb^+* controls.

same manner. AG1478 was dissolved in sterile-filtered DMSO to a final concentration of 200 mM. The dose delivered by the pump was 12 mg·kg^{-1}·d^{-1} for an average of 30 g per mouse. AG1478 has a short half-life (<60 min) in vivo (43, 44), but has been shown to successfully inhibit EGFR activity with continuous infusion at similar concentrations (45). Twenty-five mice were treated with AG1487 and 25 mice were treated with vehicle, although a few mice were lost due to normal age-related attrition. Surviving mice were harvested at age 10.5 mo. On gross examination of activity level and weight, treated and untreated mice remained indistinguishable throughout the treatment. Importantly, given the numbers of AG1478-treated eyes without glaucoma, at the reported dose there was no evidence of overt overall toxicity of AG1478 to mouse eyes.

Results

WLD^S Mitigates RGC Dysfunction in D2 Mice. D2 mice develop glaucoma with age owing to chronic IOP elevation (27, 36). Despite elevated IOP, D2 mice that express the *Wld^s* allele (D2.*Wld^s*) are protected from glaucoma, with many mice (~70% of eyes) developing no classic signs of glaucoma (20) (Fig. 1). Homozygous *Wld^s* mice had a substantially lower incidence of glaucoma compared with wild type mice, but were not more protected than heterozygous mice (Fig. 1). In D2 mice, high IOP and age are also risk factors associated with RGC dysfunction that precede overt axon loss and glaucoma. Types of RGC dysfunction include sectorial axon transport deficits, discrete axonal swellings in the ONH, and dendrite retraction (20, 40, 46–49) (Fig. 1). In D2.*Wld^s* mice with no detectable axon loss (Fig. 1 *A* and *B*), no sectorial deficits in anterograde transport of a fluorescent-labeled tracer to the superior colliculus were observed (Fig. 1*C*). D2.*Wld^s* mice also had significantly fewer ax-

onal swellings in the ONH as assessed by immunohistochemistry (Fig. 1*D*). Finally, RGC dendrites in D2.*Wld^s* mice did not atrophy, but instead remained similar to healthy controls in mean field area and complexity (Fig. 2). These changes are consistent with the preservation of PERG amplitude, a functional measure of health, in D2.*Wld^s* mice (20). This makes protected D2.*Wld^s* mice an important resource for evaluating changes that occur in the ONH in response to IOP elevation. Importantly, these mice
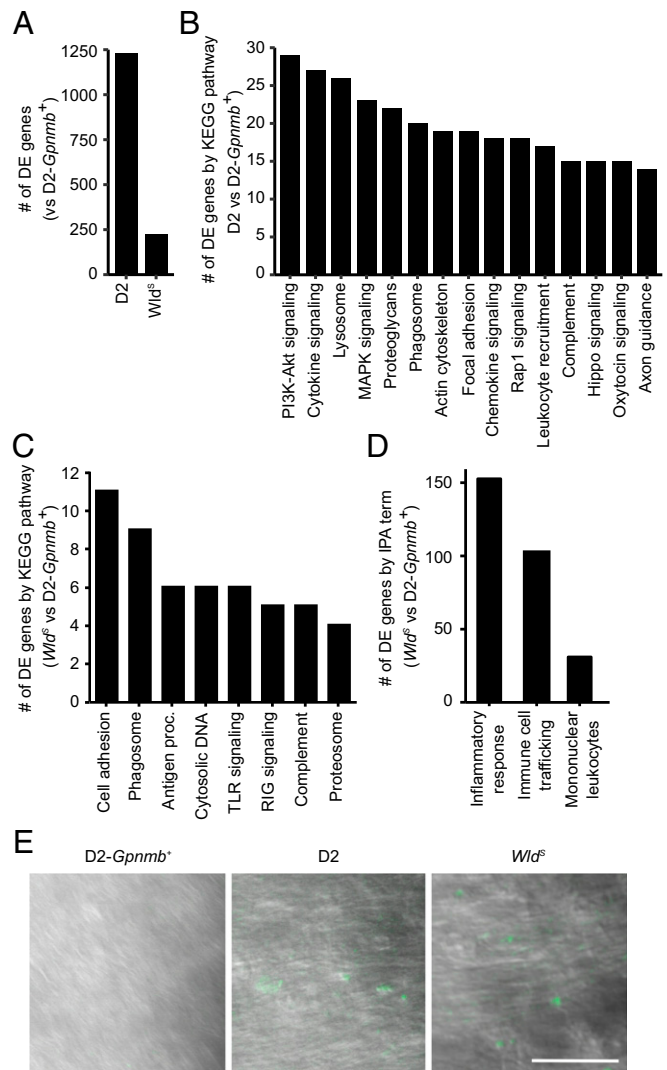

Fig. 3. Inflammatory pathways are up-regulated in D2.*Wld^s* eyes. (*A*) The number of differentially expressed genes in retinas from D2 and D2.*Wld^s* mice compared with D2.*Gpnmb^+* controls. (*B*) The top-15 enriched KEGG pathways (by gene number) comparing differentially expressed genes from D2 vs. D2.*Gpnmb^+* samples (details in Dataset S3). (*C*) Gene expression profiles of ONH tissue were compared between D2.*Wld^s* and D2.*Gpnmb^+* mice. DE genes fell into eight significantly enriched KEGG pathways (*P* ≤ 0.02 for each). Antigen proc., antigen processing and presentation; cell adhesion, cell adhesion molecules; complement, complement and coagulation pathways; cytosolic DNA, cytosolic DNA-sensing pathway; TLR signaling, Toll-like receptor signaling pathway; RIG signaling, RIG-I–like receptor signaling pathway. (*D*) By IPA, DE genes identified in the D2.*Wld^s* ONH dataset are related to inflammatory responses and immune cell infiltration. (*E*) Infiltration of peripheral immune cells (fluorescently labeled by CFDA injection into the spleen, green; *Materials and Methods*) was observed in the ONHs of all D2 and D2.*Wld^s* mice, but not in those of D2.*Gpnmb^+* mice (*n* = 10 eyes per sample group). (Scale bar: 50 µm.)
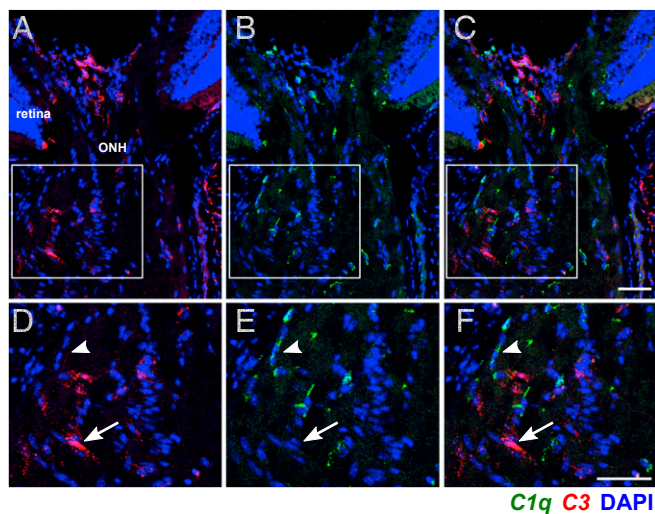
Fig. 4. *C3* and *C1q* are not expressed in the same ONH cells. Expression patterns of *C3* (red) and *C1qa* (green) were determined using two-color RNA in situ hybridization (*Materials and Methods*). (*A–C*) Examples of ONHs from a 10-mo-old D2 mouse with NOE glaucoma showing that *C3* did not colocalize with *C1qa*. (*D–F*) Magnified images from boxed regions in *A–C* showing specific cells expressing either *C3* (arrow) or *C1qa* (arrowhead). Cell nuclei are labeled with DAPI (blue). (Scale bars: 50 μm.)

allow for the identification of changes that precede these known measures of RGC dysfunction.

Immune Responses Occur in D2.Wld^s Mice. We used gene expression profiling to identify molecular changes occurring in the ONH following IOP elevation. Given the increased health of RGCs in D2.*Wld^s* mice, we reasoned that their inclusion would help us identify molecular changes resulting from high IOP as opposed to downstream consequences of RGC dysfunction. As a control, we used D2-*Gpnmb$^+$* mice, a genetically matched substrain of D2 that does not develop high IOP or glaucoma (37). D2 mice develop glaucoma owing in part to a loss-of-function mutation in *Gpnmb* that causes iris pigment dispersion in the anterior segment of the eye (37). D2 mice with functional alleles of *Gpnmb* (D2-*Gpnmb$^+$*) do not develop high IOP and maintain healthy RGCs and optic nerves.

Transcriptional profiles of ONH tissue from age- and sex-matched D2, D2.*Wld^s*, and D2-*Gpnmb$^+$* mice were generated by RNA-seq (*Materials and Methods*). Compared with D2-*Gpnmb$^+$* mice, D2.*Wld^s* mice had 5.5-fold fewer DE genes (FDR < 0.1) than D2 mice (Fig. 3*A* and Datasets S1 and S2), suggesting a less complex response to elevated IOP in D2.*Wld^s* mice than in D2 mice. We assessed the functional implications in these two DE gene sets via pathway enrichment analysis. For D2 mice, 29 Kyoto Encyclopedia of Genes and Genomes (KEGG) pathways were enriched (Fig. 3*B* and Dataset S3), including pathways known to be associated with immune cell activation, signal transduction, and neuroglial signaling. In contrast, for D2.*Wlds* mice, only eight KEGG pathways were enriched, all of which are associated with immune cell activation (Fig. 3*C*). Importantly, genes in neuroglial signaling pathways were only minimally present in the DE genes from the D2.*Wld^s* data (with only 8 of 224 DE genes relating to axon guidance and neurotrophin signaling). These data are consistent with our physiological data, and suggest that elevated IOP does not induce major RGC dysfunction in D2.*Wld^s* mice.

To confirm the finding of neuroglial related signaling in D2 mice, we updated our previously published gene expression profiling datasets of ONHs from D2 and D2-*Gpnmb$^+$* mice with

the latest KEGG pathway annotations (5, 8) (Datasets S4–S7). These previous studies used a large cohort of D2 mice to define molecular stages of glaucoma that preceded conventional morphological measures of damage (termed predegenerative stages 1a, 1b, 1c, and 2) (5, 8). The updated analyses indicated that, in addition to the many immune-related changes, altered neuroglial signaling (125 genes in axon guidance, ID: 4360; neurotrophin signaling, ID: 4722) occurs during predegenerative stages of glaucoma.

We further defined the type of immune responses occurring in D2.*Wld^s* mice using Ingenuity Pathway Analysis (IPA). IPA associated 150 of the 224 genes that are DE in D2.*Wld^s* mice with the term "inflammatory response" (Fig. 3*D*). The majority of these genes were associated with "immune cell trafficking." Furthermore, the molecular signature of "mononuclear leukocytes"
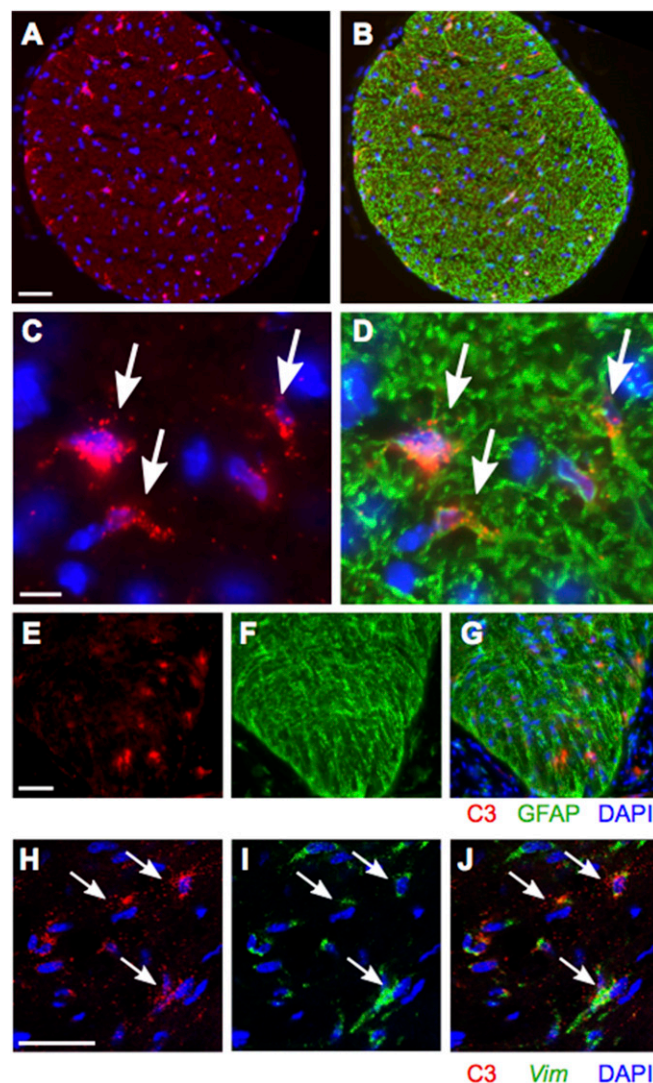

Fig. 5. C3 colocalizes with GFAP and vimentin (*Vim*) in the ONHs of D2 mice. (*A* and *B*) FISH (red) combined with immunofluorescence (green) in a cross-section of ONH tissue showing coexpression of C3 (red) and GFAP (green; astrocyte marker). (*C* and *D*) Magnified images showing coexpression of C3 and GFAP in the same cells. (*E* and *F*) FISH for C3 in longitudinal sections of the ONH showing C3 expression directly behind the eye. (*H* and *J*) Two-color RNA in situ hybridization-stained ONH longitudinal sections showing colocalization of vimentin (*Vim*, a specific marker of ONH astrocytes) and C3 (arrows). (Scale bars: 50 μm in *A* and *B*; 10 μm in *C* and *D*; 50 μm in *E–G*; 50 μm in *H–J*.)
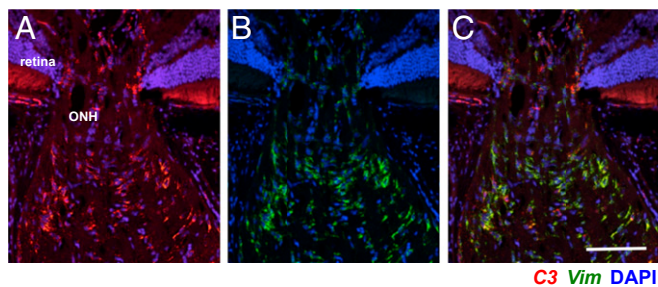
Fig. 6. C3 colocalizes with vimentin (*Vim*) in ONHs of D2.*Wld^s* mice. Representative FISH images with probes for *C3* (red) and *Vim* (green) showing colocalization in an ONH from a 10-mo-old D2.*Wld^s* mouse. Cell nuclei are labeled with DAPI (blue). Magnified images show cells with overlapping expression of *C3* and *Vim*. (Scale bar: 50 μm.)

suggested that peripherally derived immune cells were recruited to the ONH in D2.*Wld^s* mice, as was the case for D2 mice (5). To confirm leukocyte infiltration in D2.*Wld^s* mice, 6-CFDA (a fluorescent tracer for infiltrating cells) (5) was injected into the spleens of D2.*Wld^s*, D2, and D2-*Gpnmb^+* mice. Three days later, 6-CFDA^+ cells were observed in the ONH of D2.*Wld^s* and D2 mice, but not in that of D2-*Gpnmb^+* mice (Fig. 3*E*). Taken together, these results suggest that immune responses that include the recruitment of peripheral immune cells occur as a result of high IOP in D2.*Wld^s* mice. The immune response occurred in D2.*Wld^s* mice even in the absence of detectable RGC dysfunction assessed using various physiological, cell biological, and molecular approaches.

Up-Regulation of Complement Component C3 Is an Early Immune Response in the ONH of D2.*Wld^s* and D2 Mice. We next compared the KEGG pathways overrepresented in the D2.*Wld^s* data with the pathways overrepresented in each D2 dataset to identify common pathways that may be altered due to IOP elevation. Phagosome-related genes were altered in the D2.*Wld^s* and D2 RNA-seq data (Fig. 3 *B* and *C*) and in the earliest molecular

stages (stages 1a and 1b) of our previous D2 data (5), including opsonins, phagocytic receptors, lysosomal membrane components, and lysosomal enzymes (Fig. S1). The earliest opsonin significantly up-regulated in each dataset was the complement component 3 (*C3*; D2.*Wld^s*, +1.9-fold; D2, +1.4-fold; D2 stage 1a, +3.9-fold; D2 stage 1b, +3.3-fold). Complement activation has been identified in human glaucoma (50, 51), and components of the complement cascade are known to mediate RGC loss and optic nerve degeneration in D2 glaucoma (8, 51, 52). In support of an important role for C3 effector fragments (C3a and C3b) during early stages of glaucoma, expression of a C3a receptor (*C3ar1*), a C3b receptor (CR4 receptor consisting of an *Itgax* and *Itgb2* dimer), and the alternative pathway component C3 convertase (*Cfb*) were increased in glaucoma stage 1a and all subsequent stages (Fig. S2).

C3 Is Induced in Astrocytes, but Not Myeloid Cells, in the ONH in D2 Glaucoma. To better understand the role of C3 in glaucoma, we used RNA in situ hybridization to identify the specific cell types expressing C3 transcripts. We previously reported *C1qa* expression in IBA1^+ myeloid cells (microglia/monocytes) and RGCs (8). In contrast, colabeling of ONH sections from at least six D2 eyes with riboprobes for *C1qa* and *C3* showed no observable colocalization (Fig. 4). This suggests that myeloid cells in the ONH do not express C3. However, C3 expression was expressed in GFAP^+ and *Vim^+* astrocytes (Fig. 5). C3 also was expressed by *Vim^+* astrocytes in D2.*Wld^s* eyes (Fig. 6). Although we saw no evidence of C3 expressed in ONH cells other than astrocytes, we cannot rule out transient expression in additional cell types. C3 was not constitutively expressed by all astrocytes, and the number of C3-expressing astrocytes varied among eyes. C3 expression was assessed in at least 10 DBA/2J eyes with NOE glaucoma (encompassing all predegenerative stages), and similar numbers of D2.*Wld^s* eyes. The degree of C3 expression varied between eyes with NOE glaucoma and between D2.*Wld^s* eyes. According to our previously reported microarray-based gene expression study, unclustered NOE samples showed varying levels of expression of C3 (5, 8), similar to the findings reported here. In contrast, C3 expression generally increases from stages
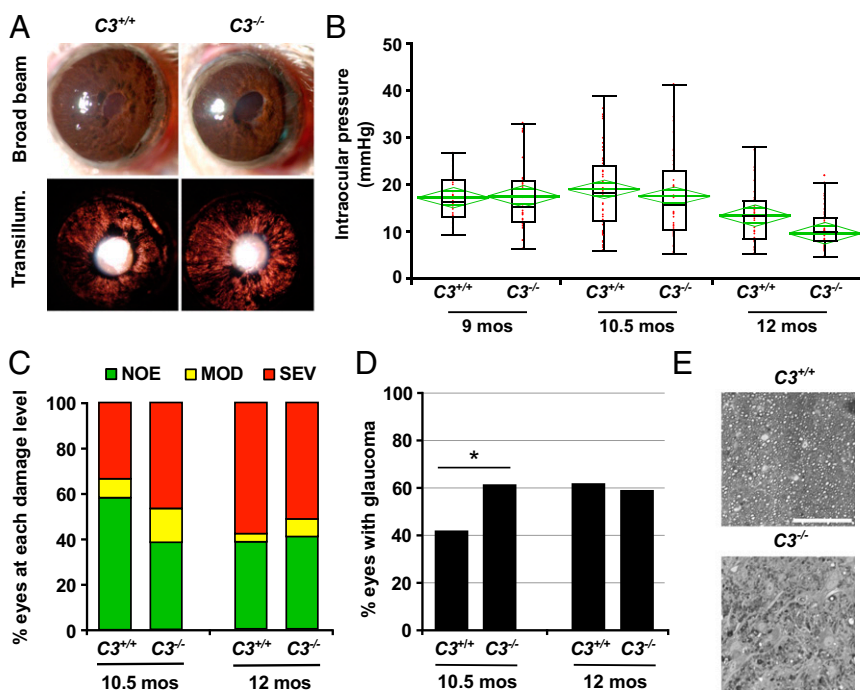

Fig. 7. C3 is protective in early D2 glaucoma. (*A*) D2. C3^−/− mice developed iris disease without difference to standard D2 mice. Depigmentation of the iris was observed both by broad-beam illumination (*Upper*) and transillumination (*Lower*). (*B*) Age-dependent elevation of IOP was observed in both C3-sufficient D2 (*C3^+/+*) and C3-deficient D2 (*C3^−/−*) mice, present in a subset of eyes at age 9 mo. There were no significant differences between genotypes at each age assessed (8.5–9.0 mo, *P* = 0.88; 10–10.5 mo, *P* = 0.92; 12–12.5 mo, *P* = 0.94). Boxplots were generated using JMP version 7.0. The boxes define the 75th and 25th percentiles, and the black line in the middle of each box represents the median value. The whiskers depict the full range of the data points. The green diamonds indicate the mean value and the 95% CI. (*C* and *D*) Optic nerve damage was significantly increased in *C3^−/−* mice compared with *C3^+/+* mice at age 10.5 mo. Bars represent the distribution of optic nerve damage by genotype and age. At age 10.5 mo, *C3^−/−* mice exhibited significantly increased nerve damage (*P* = 0.01). (*E*) Examples of the most common damage level for *C3^+/+* (NOE) and C3^−/− (SEV) at age 10.5 mo. (Scale bar: 50 μm.)
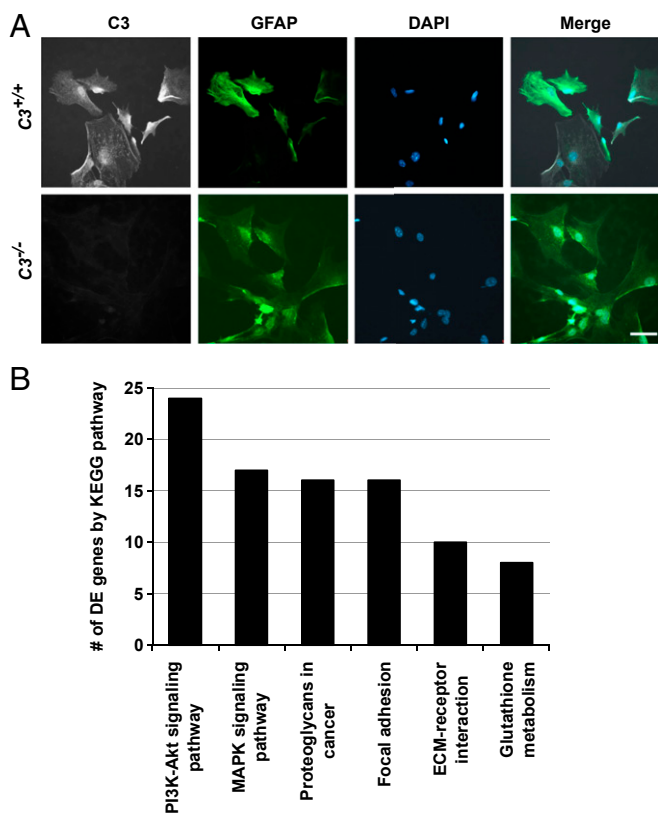
Fig. 8. C3 deficiency perturbs multiple cell signaling pathways in cultured cortical astrocytes. (*A*) Cultured GFAP$^+$ cortical astrocytes from D2 (*C3$^{+/+}$*) mice express C3 (*Upper*), but those from C3-deficient (*C3$^{-/-}$*) D2 mice do not (*Lower*). (*B*) Bar chart showing the number of DE genes in enriched KEGG pathways between cultured astrocytes (GFAP^{hi}, selected by FACs) from *C3*-sufficient (*C3$^{+/+}$*) and *C3*-deficient (*C3$^{-/-}$*) mice.

1a through stage 2 in clustered samples (stage 1a, +3.8-fold; stage 1b, +3.3-fold, stage 1c, +3.9-fold; stage 2, +5.9-fold) (5, 8). Given that clustering of gene expression profiles is a much more sensitive measure of expression levels during early glaucoma than RNA in situ hybridization, these data suggest that expression of C3 in the ONH increases with early molecular disease progression and before axon degeneration. Furthermore, although more work is needed, C3 may be a marker of ONH astrocytes that are

actively responding to local biological stresses or increased mechanical strain.

C3 Is Protective in Early D2 Glaucoma. To functionally test the role of C3 in glaucoma, a null allele of *C3* was backcrossed into the D2 strain (D2.*C3$^-$*) and then intercrossed to generate C3-deficient (D2.*C3$^{-/-}$*) mice and C3-sufficient (D2.*C3$^{+/+}$*; regular D2) littermate controls. Ocular examinations were performed to assess the effects of *C3* deficiency on iris disease (Fig. 7*A*). D2.*C3$^{+/+}$* and D2.*C3$^{-/-}$* eyes evaluated at 6, 8, 10, and 12 mo exhibited the hallmark iris disease with no obvious differences in onset or progression. Ocular hypertension in D2.*C3$^{+/+}$* and D2.*C3$^{-/-}$* eyes also occurred in the characteristic pattern associated with D2 glaucoma (Fig. 7*B*). In our colony, most D2 eyes develop optic nerve degeneration and RGC loss between 10 and 12 mo. Surprisingly (because *C1qa* deficiency decreases glaucoma in D2 eyes) (8), significantly more D2.*C3$^{-/-}$* eyes than D2.*C3$^{+/+}$* eyes had severe optic nerve damage at 10.5 mo (Fig. 7 *C–E*). Given that D2.*C3$^{-/-}$* mice have similar IOP profiles as control mice, the greater incidence of nerve damage in D2.*C3$^{-/-}$* mice indicates that C3 deficiency increases the probability or risk of degeneration due to elevated IOP at 10.5 mo. By 12 mo, similar numbers of D2.*C3$^{+/+}$* and D2.*C3$^{-/-}$* eyes had severe axon loss. Therefore, the total number of D2 eyes ultimately developing glaucoma within the window of IOP insult (~8–12 mo for most mice in our colony) is not impacted by C3 deficiency. Collectively, the 10.5- and 12-mo data suggest that longer-term IOP elevation and its associated stresses induce damaging processes that overcome the early protective effects of C3.

In D2 glaucoma, apoptosis of RGC somas can be uncoupled from axon degeneration, with specific molecules having differential effects on axons and somas (39). There is no evidence that C3 deficiency differentially affects RGC axons and somas; for example, C3-deficient eyes with severe axon loss also have severe soma loss (Fig. S3). In summary, loss of C3 increased the probability of nerve damage, axon loss, and soma loss early in glaucoma. Taken together, our data suggest that in response to high IOP-induced stress, astrocytes in the ONH produce C3 to support RGC survival.

C3 Genotype Modulates EGFR Signaling in Cultured Astrocytes. To better understand the effects of *C3* deficiency, we generated C3-sufficient and C3-deficient astrocyte cultures. Cultured neonatal cortical astrocytes are more like astrocytes responding to a stress stimulus in vivo than like astrocytes in a normal, healthy environment (53); therefore, this culture model is relevant for

Fig. 9. Network analyses identified EGFR as a hub in the astrocytic network of genes perturbed by C3 deficiency. (*A*) Venn diagram displaying the number of genes that are unique and overlap in three cell signaling pathways altered by C3 deficiency in cultured astrocytes (shown in Fig. 6*C*). Only three DE genes are common among the three pathways: *Egfr*, *Fgf14*, and *Fgf18*. (*B*) Network interaction diagram (created using STRING) depicting known and predicted protein interactions of genes in the MAPK signaling, PI3K-AKT signaling, and proteoglycans in cancer pathways. Node colors correspond to the Venn diagram colors in *A*, with additional colors representing genes in multiple pathways. Purple indicates genes shared by PI3K-AKT and MAPK signaling, orange indicates genes shared by the PI3K-AKT and proteoglycan pathways, green indicates genes shared by the MAPK and proteoglycan pathways, and brown indicates genes

shared by all of the pathways. Gray lines indicate protein interactions, and black lines indicate protein interactions with EGFR. Among the three genes common to the three pathways, *Egfr* encodes the protein that interacts with the largest number of proteins in the network.
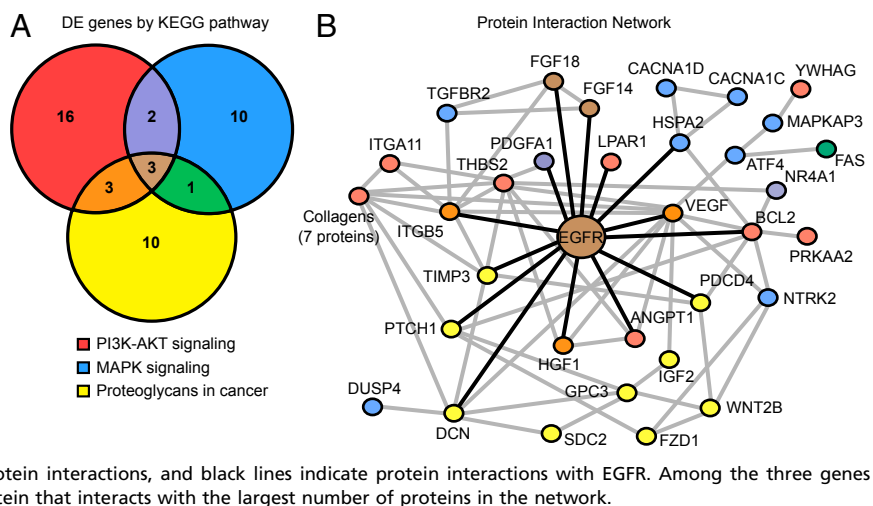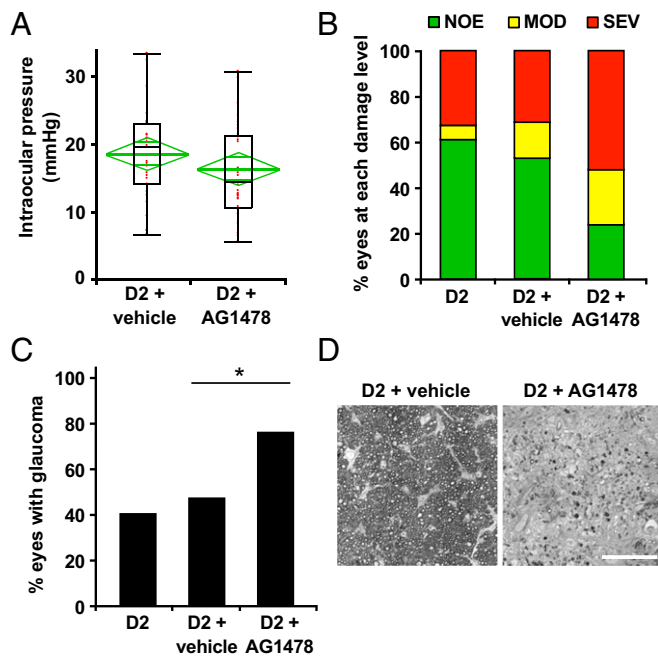
Fig. 10. Continuous administration of EGFR inhibitor AG1478 increases neurodegeneration in DBA/2J mice. AG1478 or vehicle was administered to D2 mice from age 7 mo to 10.5 mo using an mini osmotic pump (*Materials and Methods*), and IOP and glaucoma were assessed. (*A*) Age-dependent elevation of IOP was found in both vehicle-treated and AG1478-treated D2 mice at age 10.5 mo. No significant differences were observed based on treatment ($P = 0.08$). Boxplot parameters are described in the Fig. 7 legend. (*B* and *C*) Optic nerve damage distributions for three cohorts of mice: untreated (D2), DMSO-treated (D2 + vehicle), and AG1478-treated (D2 + AG1478). By age 10.5 mo, a significant increase in optic nerve damage was observed in the AG1478-treated mice compared with either the D2 mice or vehicle-treated mice (3×3 Fisher exact test, $P = 0.004$; Fisher exact test comparing AG1478 with vehicle, $P = 0.01$). (*D*) Examples of the most common damage levels for vehicle-treated (NOE; *Left*) and AG1478-treated (SEV; *Right*) mice. (Scale bar: 50 μm.)

studying astrocytic C3 function. Primary cultures of D2.$C3^{+/+}$ astrocytes expressed C3 as detected by immunofluorescence (Fig. 8*A*). As expected, C3 was absent in astrocytes from D2.$C3^{-/-}$ mice (Fig. 8*A*).

We transcriptionally profiled C3-deficient and C3-sufficient astrocytes by RNA-seq. Comparing profiles from these two groups identified a total of 548 DE genes (Dataset S8). As expected, C3-deficient astrocytes produced a mutant allele of the C3 transcript (Dataset S8) that is unable to form the C3a and C3b protein fragments (54). Enrichment analysis identified three significantly overrepresented KEGG pathways (containing 45 of the 548 DE genes) (Fig. 8*B*). Two of these pathways are related to signal transduction in response to extracellular signaling: PI3K-AKT signaling and MAPK signaling. The third pathway is an inflammatory signaling pathway, proteoglycans in cancer. All three pathways were overrepresented in the D2 RNA-seq data (Fig. 3*B*) and in the earliest predegenerative glaucoma stages 1a and 1b (Datasets S4 and S5). Only three genes (*Egfr*, *Fgf14*, and *Fgf18*) were common to all three pathways, suggesting that they may be master regulators (Fig. 9*A*). STRING network analysis showed that EGFR interacts directly with 14 of these 45 DE genes (compared with only three for FGF14 and three for FGF18) (Fig. 7*B*), predicting EGFR as a key hub in the network (Fig. 9*B*). Given that EGFR activation has been shown in astrocytes after IOP elevation (55–57), these data are consistent with a C3-dependent astrocytic response that involves EGFR signaling.

Treatment with EGFR Inhibitor AG1478 Increases Nerve Damage in Early Glaucoma. To assess the role of EGFR signaling in glaucoma, we first assessed a downstream target of EGFR signaling. Transactivation of EGFR signaling (e.g., via LPAR1, which is expressed by astrocytes) (Fig. 9*B*) induces increased expression of cytosolic phospholipase A2 (cPLA2) enzymes (58–61). In our gene expression data, the cPLA2 enzyme *Pla2g4a* was up-regulated by 1.476-fold in early glaucoma (stage 1b; $P = 0.0004$), and RNA in situ hybridization revealed its expression by astrocytes in the ONH (Fig. S4).

Next, to functionally test the role of EGFR signaling, we pharmacologically prevented EGFR activation using AG1478, an EGFR inhibitor (62). AG1478 was administered by a mini osmotic pump beginning at 7 mo (before the onset of IOP elevation in most eyes), and glaucoma was assessed at 10.5 mo. A control group of mice were administered DMSO alone (vehicle). Ocular examinations were performed to assess iris disease and IOP elevation. There were no significant differences in the development of iris disease (not shown) or IOP profiles (Fig. 10) between treated and vehicle groups at 10.5 mo; however, EGFR inhibition substantially increased the numbers of eyes with moderate or severe glaucoma. Glaucomatous optic nerve damage was seen in 80% of AG1478-treated mice, compared with only 40% of vehicle-treated and untreated controls (Fig. 10).

Collectively, these data indicate that C3 and EGFR signaling are involved in a protective response in glaucoma. This response appears to be mediated by astrocytes as a direct result of IOP elevation and before detectable RGC dysfunction/damage occurs.

Discussion

Age-related neurodegenerative diseases, including glaucoma, can involve complex interactions among neurons, glial cells, the vasculature, and the immune system (63). In glaucoma, RGCs and the optic nerve degenerate subsequent to IOP elevation, RGC dysfunction, and immune responses (5–9). Here we identified neuroglial and phagosome pathways as additional processes altered before RGC degeneration and a potential component of pathological changes in glaucoma. To understand these early disease processes, we performed transcriptional profiling in ONH tissue from D2.Wld^s mice. We found that D2.Wld^s mice are protected from detectable axon damage and RGC dysfunction, changes that are clearly evident in D2 mice. In response to elevated IOP, D2.Wld^s mice were protected from the transcriptional changes related to the neuroglial interactions seen in D2 mice, but did show changes in expression of immune response genes, including innate immune signaling and phagosome pathways. These changes included recruitment of peripheral immune cells and up-regulation of components of the complement cascade, including C3. These data demonstrate that the initial immune responses in glaucoma are not secondary to the assessed measures of neuronal dysfunction and likely are induced directly as a result of high IOP. We have previously shown that these immune responses include infiltration of damaging monocytes, a process necessary for the death of RGCs (5). Using D2.$Wlds$ mice, we now suggest that these immune responses also include a beneficial response by C3-expressing astrocytes.

Our experiments suggest that the classic immune molecule C3 modulates a beneficial response during early stages of glaucoma. Elevated C3 expression persists at later stages of glaucoma (Fig. S2), suggesting that this early beneficial response might not be transient, but ultimately is not sufficient to prevent more damaging processes from occurring. Our understanding of the role of C3 in astrocytes in glaucoma and other neurodegenerative diseases remains incomplete, however. C3 activation can promote cell lysis through downstream activation of complement components 5–9 (C5–C9) and formation of the membrane attack complex (MAC). D2 mice are C5-deficient due to a natural

mutation, and the MAC is not detectable in D2 glaucoma (52). When C5 is expressed in D2 mice, deposition of the MAC corresponds with worsening glaucoma (52); thus, the protective function of C3 in glaucoma likely is not related to the promotion of MAC formation. Other functions of C3 include promoting phagocytosis, cell adhesion, and chemotaxis. Both phagocytosis and cell infiltration are implicated in glaucoma (5, 41, 64, 65). Given the physiological function of ONH astrocytes in phagocytosing myelin and mitochondria, an early effect of high IOP may be to alter astrogliosis and disrupt phagocytosis (41, 66). These functions are carried out when C3 effector fragments bind various receptors, including C3AR1 for C3a and CR1, CR2, CR3, and CR4 for C3b (67). Manipulating C3 receptors will help determine the specific C3 fragments and cellular process that mediate its neuroprotective functions.

In contrast to our findings for *C3*, deletion of *C1qa* prevents RGC loss in glaucoma (8, 68). Similar results have been shown in another neurodegenerative disease; in mouse models of Alzheimer's disease, *C1qa* deficiency was protective (69), whereas *C3* deficiency accelerated aspects of the disease (70). These data suggest that in neurodegenerative diseases, some functions of *C1q* and *C3* may be independent. This idea is supported by the differential expression of *C1qa* and *C3* in different cell types in the ONH (Fig. 3). The nature of these independent roles is not clear, however. The complement cascade can be activated through three different pathways: the classical, alternative, and lectin pathways. The classical pathway is initiated by formation of the C1 complex that includes complement components C1q (comprising C1qa, C1qb, and C1qc subunits), C1s, and C1r. Formation of the C1 complex can lead to the cleavage of C3 to C3 effector fragments; however, C3 effector fragments can be generated independently of the C1 complex through the alternative or the lectin pathways. Conversely, the C1 complex, or genes that make up the C1 complex, such as *C1qa*, can act independently of C3 through a variety of different interactions (reviewed in ref. 71). The C1 complex can bind receptors that affect immune cell differentiation and polarization (71) or compete with binding of opsonins (including C3) to phagocytic receptors and interfere with efficient phagocytosis (72, 73). The C1q subunit, comprising C1qa, C1qb, and C1qc, has a collagen-like domain that can stabilize immune complex formation in the basement membrane (74). Given that multiple studies have shown alterations to extracellular matrix proteins in the ONH in human and animals models of glaucoma (reviewed in refs. 1, 2), and immune cells are known to infiltrate into the ONH during early stages of glaucoma (5), the possibility of C1q mediating localization and/or immune cell responses in the ONH is intriguing. Overall, the significant yet divergent impact of complement cascade manipulations in neurodegenerative disease warrants further investigation. It will be important to determine the roles of specific complement components in glaucoma by cell type, and also to assess additional pathways of C3 activation, targets of C1 (e.g., C4), and the roles of specific C1q complement receptors (e.g., CR1).

Our data are consistent with beneficial actions of C3 and EGFR against glaucoma, and suggest that C3 and EGFR signaling are part of an integrated response rather than two pathways working independently. Both *C3* and *Egfr* are expressed by astrocytes in the ONH (55, 56) (Figs. 4–6). Our analyses using cultured astrocytes have shown that a deficiency of C3 affects the expression of major signal transduction pathways that involve EGFR, including MAPK signaling, PI3K-AKT signaling, and proteoglycan signaling (Fig. 6B). The similar effect of a loss of C3 or EGFR may be mediated through a shared target; C3 receptors and EGFR have common downstream targets, among them the MAP kinases (75–77). Although our collective data support protective roles for C3 and EGFR in early glaucoma, further studies are needed to confirm the relationship between C3 and EGFR and to identify the upstream and downstream components of this beneficial process. Administration of AG1478 increased the rate of nerve damage from 40% to 80% at 10.5 mo. Although AG1478 is an effective EGFR inhibitor in vivo (78, 79), as with many kinase inhibitors, off-target and systemic effects are possible. AG1478 is less effective in inhibiting other inflammation-related kinases (80). Therefore, although our data support a beneficial role of EGFR, specific depletion of *Egfr* in astrocytes is required to definitively show that EGFR in astrocytes is neuroprotective.

This paper contributes to a model in which immune-like responses by multiple cell types, including astrocytes, microglia, and infiltrating monocytes, occur early in glaucoma and are not dependent on RGC dysfunction and axon damage. Our previous work shows that monocytes infiltrate into the ONH before RGC loss, a process that is apparently damaging to RGCs (5). The data presented here suggest that other immune responses, likely mediated by astrocytes, are protective. Although the exact timing and sequencing of responses has not been determined, our data support the idea that the beneficial response is triggered as a direct result of IOP elevation. Although this initial response is protective, over the course of this chronic disease, aspects of these immune responses ultimately become damaging to RGCs. This model suggests that wholesale inhibition of complement-mediated immune responses is not a viable strategy for treatment of human glaucoma.

1. Burgoyne CF (2011) A biomechanical paradigm for axonal insult within the optic nerve head in aging and glaucoma. *Exp Eye Res* 93:120–132.
2. Nickells RW, Howell GR, Soto I, John SW (2012) Under pressure: Cellular and molecular responses during glaucoma, a common neurodegeneration with axonopathy. *Annu Rev Neurosci* 35:153–179.
3. Quigley HA (1996) Number of people with glaucoma worldwide. *Br J Ophthalmol* 80:389–393.
4. Leske MC, Wu SY, Hennis A, Honkanen R, Nemesure B; BESs Study Group (2008) Risk factors for incident open-angle glaucoma: The Barbados Eye Studies. *Ophthalmology* 115:85–93.
5. Howell GR, et al. (2012) Radiation treatment inhibits monocyte entry into the optic nerve head and prevents neuronal damage in a mouse model of glaucoma. *J Clin Invest* 122:1246–1261.
6. Tezel G, et al. (2007) Mechanisms of immune system activation in glaucoma: Oxidative stress-stimulated antigen presentation by the retina and optic nerve head glia. *Invest Ophthalmol Vis Sci* 48:705–714.
7. Hernandez MR, Pena JD (1997) The optic nerve head in glaucomatous optic neuropathy. *Arch Ophthalmol* 115:389–395.
8. Howell GR, et al. (2011) Molecular clustering identifies complement and endothelin induction as early events in a mouse model of glaucoma. *J Clin Invest* 121:1429–1444.
9. Kong YX, Crowston JG, Vingrys AJ, Trounce IA, Bui VB (2009) Functional changes in the retina during and after acute intraocular pressure elevation in mice. *Invest Ophthalmol Vis Sci* 50:5732–5740.
10. Phani S, Loike JD, Przedborski S (2012) Neurodegeneration and inflammation in Parkinson's disease. *Parkinsonism Relat Disord* 18:S207–S209.
11. Heneka MT, et al. (2015) Neuroinflammation in Alzheimer's disease. *Lancet Neurol* 14:388–405.
12. Crotti A, Glass CK (2015) The choreography of neuroinflammation in Huntington's disease. *Trends Immunol* 36:364–373.
13. Soto I, Howell GR (2014) The complex role of neuroinflammation in glaucoma. *Cold Spring Harb Perspect Med* 4:a017269.
14. Tezel G (2011) The immune response in glaucoma: A perspective on the roles of oxidative stress. *Exp Eye Res* 93:178–186.
15. Johnson EC, Morrison JC (2009) Friend or foe? Resolving the impact of glial responses in glaucoma. *J Glaucoma* 18:341–353.
16. Quigley HA, Anderson DR (1977) Distribution of axonal transport blockade by acute intraocular pressure elevation in the primate optic nerve head. *Invest Ophthalmol Vis Sci* 16:640–644.
17. Quigley H, Anderson DR (1976) The dynamics and location of axonal transport blockade by acute intraocular pressure elevation in primate optic nerve. *Invest Ophthalmol* 15:606–616.

18. Anderson DR, Hendrickson A (1974) Effect of intraocular pressure on rapid axoplasmic transport in monkey optic nerve. *Invest Ophthalmol* 13:771–783.
19. Quigley HA, Flower RW, Addicks EM, McLeod DS (1980) The mechanism of optic nerve damage in experimental acute intraocular pressure elevation. *Invest Ophthalmol Vis Sci* 19:505–517.
20. Howell GR, et al. (2007) Axons of retinal ganglion cells are insulted in the optic nerve early in DBA/2J glaucoma. *J Cell Biol* 179:1523–1537.
21. Burgoyne CF, Downs JC, Bellezza AJ, Suh JK, Hart RT (2005) The optic nerve head as a biomechanical structure: A new paradigm for understanding the role of IOP-related stress and strain in the pathophysiology of glaucomatous optic nerve head damage. *Prog Retin Eye Res* 24:39–73.
22. Sigal IA, Flanagan JG, Tertinegg I, Ethier CR (2004) Finite element modeling of optic nerve head biomechanics. *Invest Ophthalmol Vis Sci* 45:4378–4387.
23. Jakobs TC (2014) Differential gene expression in glaucoma. *Cold Spring Harb Perspect Med* 4:a020636.
24. Nikolskaya T, et al. (2009) Network analysis of human glaucomatous optic nerve head astrocytes. *BMC Med Genomics* 2:24.
25. Johnson EC, Jia L, Cepurna WO, Doser TA, Morrison JC (2007) Global changes in optic nerve head gene expression after exposure to elevated intraocular pressure in a rat glaucoma model. *Invest Ophthalmol Vis Sci* 48:3161–3177.
26. John SW, et al. (1998) Essential iris atrophy, pigment dispersion, and glaucoma in DBA/2J mice. *Invest Ophthalmol Vis Sci* 39:951–962.
27. Libby RT, et al. (2005) Inherited glaucoma in DBA/2J mice: Pertinent disease features for studying the neurodegeneration. *Vis Neurosci* 22:637–648.
28. Wong AA, Brown RE (2013) Prevention of vision loss protects against age-related impairment in learning and memory performance in DBA/2J mice. *Front Aging Neurosci* 5:52.
29. Wong AA, Brown RE (2012) A neurobehavioral analysis of the prevention of visual impairment in the DBA/2J mouse model of glaucoma. *Invest Ophthalmol Vis Sci* 53:5956–5966.
30. Matsubara A, et al. (2006) Investigating the effect of ciliary body photodynamic therapy in a glaucoma mouse model. *Invest Ophthalmol Vis Sci* 47:2498–2507.
31. Schuettauf F, Quinto K, Naskar R, Zurakowski D (2002) Effects of anti-glaucoma medications on ganglion cell survival: The DBA/2J mouse model. *Vision Res* 42:2333–2337.
32. Porciatti V, Saleh M, Nagaraju M (2007) The pattern electroretinogram as a tool to monitor progressive retinal ganglion cell dysfunction in the DBA/2J mouse model of glaucoma. *Invest Ophthalmol Vis Sci* 48:745–751.
33. Nagaraju M, Saleh M, Porciatti V (2007) IOP-dependent retinal ganglion cell dysfunction in glaucomatous DBA/2J mice. *Invest Ophthalmol Vis Sci* 48:4573–4579.
34. Smith RS, et al. (2000) Haploinsufficiency of the transcription factors FOXC1 and FOXC2 results in aberrant ocular development. *Hum Mol Genet* 9:1021–1032.
35. Anderson MG, et al. (2002) Mutations in genes encoding melanosomal proteins cause pigmentary glaucoma in DBA/2J mice. *Nat Genet* 30:81–85.
36. Chang B, et al. (1999) Interacting loci cause severe iris atrophy and glaucoma in DBA/2J mice. *Nat Genet* 21:405–409.
37. Howell GR, et al. (2007) Absence of glaucoma in DBA/2J mice homozygous for wild-type versions of *Gpnmb* and *Tyrp1*. *BMC Genet* 8:45.
38. John SW, Hagaman JR, MacTaggart TE, Peng L, Smithes O (1997) Intraocular pressure in inbred mouse strains. *Invest Ophthalmol Vis Sci* 38:249–253.
39. Libby RT, et al. (2005) Susceptibility to neurodegeneration in a glaucoma is modified by Bax gene dosage. *PLoS Genet* 1:17–26.
40. Williams PA, et al. (2016) Inhibition of the classical pathway of the complement cascade prevents early dendritic and synaptic degeneration in glaucoma. *Mol Neurodegener* 11:26.
41. Nguyen JV, et al. (2011) Myelination transition zone astrocytes are constitutively phagocytic and have synuclein dependent reactivity in glaucoma. *Proc Natl Acad Sci USA* 108:1176–1181.
42. Blankenberg D, et al. (2010) Galaxy: A web-based genome analysis tool for experimentalists. *Curr Protoc Mol Biol* 89(19.10):19.10.1–19.10.21.
43. Lenferink AE, et al. (2000) Blockade of the epidermal growth factor receptor tyrosine kinase suppresses tumorigenesis in MMTV/Neu + MMTV/TGF-alpha bigenic mice. *Proc Natl Acad Sci USA* 97:9609–9614.
44. Ellis AG, et al. (2006) Preclinical analysis of the analinoquinazoline AG1478, a specific small molecule inhibitor of EGF receptor tyrosine kinase. *Biochem Pharmacol* 71:1422–1434.
45. Zhang H, et al. (2008) Heparin-binding epidermal growth factor-like growth factor signaling in flow-induced arterial remodeling. *Circ Res* 102:1275–1285.
46. Bosco A, et al. (2008) Reduced retina microglial activation and improved optic nerve integrity with minocycline treatment in the DBA/2J mouse model of glaucoma. *Invest Ophthalmol Vis Sci* 49:1437–1446.
47. Soto I, et al. (2008) Retinal ganglion cells downregulate gene expression and lose their axons within the optic nerve head in a mouse glaucoma model. *J Neurosci* 28:548–561.
48. Crish SD, Sappington RM, Inman DM, Horner PJ, Calkins DJ (2010) Distal axonopathy with structural persistence in glaucomatous neurodegeneration. *Proc Natl Acad Sci USA* 107:5196–5201.
49. Williams PA, et al. (2013) Retinal ganglion cell dendritic atrophy in DBA/2J glaucoma. *PLoS One* 8:e72282.

50. Tezel G, et al. (2010) Oxidative stress and the regulation of complement activation in human glaucoma. *Invest Ophthalmol Vis Sci* 51:5071–5082.
51. Stasi K, et al. (2006) Complement component 1Q (C1Q) upregulation in retina of murine, primate, and human glaucomatous eyes. *Invest Ophthalmol Vis Sci* 47:1024–1029.
52. Howell GR, et al. (2013) Deficiency of complement component 5 ameliorates glaucoma in DBA/2J mice. *J Neuroinflammation* 10:76.
53. Zamanian JL, et al. (2012) Genomic analysis of reactive astrogliosis. *J Neurosci* 32:6391–6410.
54. Wessels MR, et al. (1995) Studies of group B streptococcal infection in mice deficient in complement component C3 or C4 demonstrate an essential role for complement in both innate and acquired immunity. *Proc Natl Acad Sci USA* 92:11490–11494.
55. Liu B, Neufeld AH (2004) Activation of epidermal growth factor receptor causes astrocytes to form cribriform structures. *Glia* 46:153–168.
56. Liu B, Neufeld AH (2003) Activation of epidermal growth factor receptor signals induction of nitric oxide synthase-2 in human optic nerve head astrocytes in glaucomatous optic neuropathy. *Neurobiol Dis* 13:109–123.
57. Liu B, Chen H, Johns TG, Neufeld AH (2006) Epidermal growth factor receptor activation: An upstream signal for transition of quiescent astrocytes into reactive astrocytes after neural injury. *J Neurosci* 26:7532–7540.
58. Lin CC, et al. (2012) Transactivation of EGFR/PI3K/Akt involved in ATP-induced inflammatory protein expression and cell motility. *J Cell Physiol* 227:1628–1638.
59. Letsiou E, Kitsiouli E, Nakos G, Lekka ME (2011) Mild stretch activates cPLA2 in alveolar type II epithelial cells independently through the MEK/ERK and PI3K pathways. *Biochim Biophys Acta* 1811:370–376.
60. Murakami M, et al. (1998) The functions of five distinct mammalian phospholipase A2S in regulating arachidonic acid release: Type IIa and type V secretory phospholipase A2S are functionally redundant and act in concert with cytosolic phospholipase A2. *J Biol Chem* 273:14411–14423.
61. Ma L, Nagai J, Chun J, Ueda H (2013) An LPA species (18:1 LPA) plays key roles in the self-amplification of spinal LPA production in the peripheral neuropathic pain model. *Mol Pain* 9:29.
62. Osherov N, Levitzki A (1994) Epidermal growth factor-dependent activation of the src-family kinases. *Eur J Biochem* 225:1047–1053.
63. Burda JE, Sofroniew MV (2014) Reactive gliosis and the multicellular response to CNS damage and disease. *Neuron* 81:229–248.
64. Gramlich OW, et al. (2015) Adoptive transfer of immune cells from glaucomatous mice provokes retinal ganglion cell loss in recipients. *Acta Neuropathol Commun* 3:56.
65. Yang J, Patil RV, Yu H, Gordon M, Wax MB (2001) T cell subsets and sIL-2R/IL-2 levels in patients with glaucoma. *Am J Ophthalmol* 131:421–426.
66. Davis CH, et al. (2014) Transcellular degradation of axonal mitochondria. *Proc Natl Acad Sci USA* 111:9633–9638.
67. Zipfel PF, Skerka C (2009) Complement regulators and inhibitory proteins. *Nat Rev Immunol* 9:729–740.
68. Kumari R, Astafurov K, Genis A, Danias J (2015) Differential effects of C1qa ablation on glaucomatous damage in two sexes in DBA/2NNia mice. *PLoS One* 10:e0142199.
69. Fonseca MI, Zhou J, Botto M, Tenner AJ (2004) Absence of C1q leads to less neuropathology in transgenic mouse models of Alzheimer's disease. *J Neurosci* 24:6457–6465.
70. Maier M, et al. (2008) Complement C3 deficiency leads to accelerated amyloid beta plaque deposition and neurodegeneration and modulation of the microglia/macrophage phenotype in amyloid precursor protein transgenic mice. *J Neurosci* 28:6333–6341.
71. Scott D, Botto M (2016) The paradoxical roles of C1q and C3 in autoimmunity. *Immunobiology* 221:719–725.
72. Butko P, Nicholson-Weller A, Wessels MR (1999) Role of complement component C1q in the IgG-independent opsonophagocytosis of group B streptococcus. *J Immunol* 163:2761–2768.
73. Eggleton P, Reid KB, Tenner AJ (1998) C1q—how many functions? How many receptors? *Trends Cell Biol* 8:428–431.
74. Bohnsack JF, et al. (1985) The C1q subunit of the first component of complement binds to laminin: A mechanism for the deposition and retention of immune complexes in basement membrane. *Proc Natl Acad Sci USA* 82:3824–3828.
75. Monsinjon T, et al. (2003) Regulation by complement C3a and C5a anaphylatoxins of cytokine production in human umbilical vein endothelial cells. *FASEB J* 17:1003–1014.
76. Li XJ, et al. (2015) Protein-tyrosine phosphatase Shp2 positively regulates macrophage oxidative burst. *J Biol Chem* 290:3894–3909.
77. Nguyen LK, Kolch W, Kholodenko BN (2013) When ubiquitination meets phosphorylation: A systems biology perspective of EGFR/MAPK signalling. *Cell Commun Signal* 11:52.
78. Choi SK, et al. (2012) Chronic inhibition of epidermal growth factor receptor tyrosine kinase and extracellular signal-regulated kinases 1 and 2 (ERK1/2) augments vascular response to limb ischemia in type 2 diabetic mice. *Am J Pathol* 180:410–418.
79. Belmadani S, Palen DI, Gonzalez-Villalobos RA, Boulares HA, Matrougui K (2008) Elevated epidermal growth factor receptor phosphorylation induces resistance artery dysfunction in diabetic db/db mice. *Diabetes* 57:1629–1637.
80. MRC Protein Phosphorylation and Ubiquitylation Unit (2017) MRC Protein Phosphorylation and Ubiquitylation Unit International Centre for Kinase Profiling. Available at www.kinase-screen.mrc.ac.uk. Accessed January 28, 2017.